Application of the nonlinear substructuring control method to nonlinear 2-degree-of-freedom systems

Ryuta Enokida[1], David Stoten[1] and Koichi Kajiwara[2]

[1] Advanced Control and Test Laboratory, Department of Mechanical Engineering, University of Bristol, Queen's Building, University Walk, Bristol BS8 1TR, UK
[2] E-Defense, National Research Institute for Earth Science and Disaster Prevention, 1501-21 Nishikameya, Mitsuda, Shijimi-cho Miki, Hyogo, 673-0515 Japan

Corresponding author's e-mail address: re12126@bristol.ac.uk

Abstract.

A nonlinear substructuring control (NLSC) method is developed as a more generalised form of linear substructuring control (LSC) by incorporating nonlinear signal-based control (NSBC) into a dynamical substructuring system (DSS). An advantage of NLSC is that it can be designed using the linearized models of the substructured systems without the need for accurate nonlinear dynamic models. In this study, the use of the NLSC method is demonstrated via substructured tests on nonlinear physical and numerical substructures.

A series of substructuring tests were also conducted on a test rig, constructed within the ACTLab at the University of Bristol, which incorporated a pure time delay of 6.0 ms due to the presence of discrete-time elements. In the substructured tests, a trilinear hysteresis with piecewise linearity, commonly used in structural engineering, was embedded into the numerical substructure as the nonlinearity. The NLSC method was found to achieve stable and reliable substructured responses, even when the substructured systems had significant nonlinearity as well as the pure time delay term.

1. Introduction

Dynamically substructured experimentation, where a physical experiment and numerical simulation are conducted at the same time (with real-time interaction between them), in order to emulate the behaviour of a complete system, was originally developed for the examination of large specimens such as civil structures. The ideal substructured test is achievable only when the real time interaction between the physical and numerical substructures occurs over an infinitesimally short time. However, real implementations inevitably require transfer systems (i.e. actuators and measurement systems) for the interaction of the two substructures, and discrete-time elements in the transfer system (e.g. controllers and signal conditioners) result in the generation of a pure time delay. This pure time delay can have significant influence on the stability of the experimentation, even if it is generally of the order of milliseconds.

The hybrid simulation (HS) scheme is commonly used for substructured experimentation. In the HS scheme, the critical pure time delay (the maximum value to maintain stability, which is also used as an index of relative stability) is directly governed by the damping and natural frequency of the physical substructure, ω_p and ζ_p respectively. This critical pure time delay can be approximated as $2\zeta_p/\omega_p$, [1,2]. Thus, the HS scheme is problematic when physical substructures have small damping and high natural frequencies. Therefore, many compensation methods have been actively developed

for negating the effect of the pure time delay (e.g. [2-9]) in the HS scheme. Very often, investigations have assumed that the complete actuator dynamics can be modelled as a pure time delay, an assumption that is avoided in this work.

An analysis and synthesis framework for such problems, termed the dynamically substructured system (DSS) scheme, was developed from a control engineering point-of-view; [10,11]. The corresponding linear substructuring control (LSC) method, developed together with DSS in [10], was found to provide DSS with high robustness for linear systems containing pure time delay elements; [1]. This robustness results from the LSC design, where the closed-loop characteristic polynomial can be synthesised to have an arbitrarily large relative stability margin, a result that is in sharp contradistinction to the fixed margins induced by techniques such as HS (or, to use its often used misnomer, 'hardware-in-the-loop simulation'); [11].

In this study, a *nonlinear* substructuring control (NLSC) method - a more generalised form of LSC - is developed as an application of the nonlinear signal-based control method (NSBC), [12], to DSS. NSLC is examined via a substructured test of a 2-DOF system for a nonlinear base-isolated structure, as shown in Figure 1.

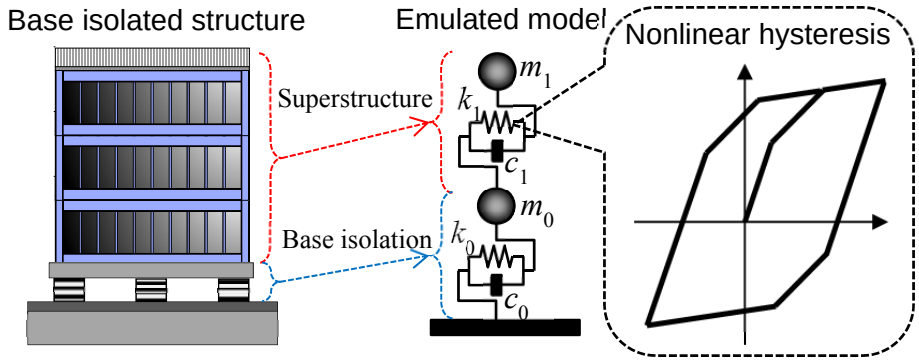

Figure 1. Dynamical substructuring test of a base-isolated structure with a rubber bearing.

2. Nonlinear substructuring control

The development of NLSC is based on NSBC [12], which utilises a 'nonlinear signal' obtained from the difference of the outputs of the nonlinear system and its linear model under the same input. In the block diagram of NLSC shown in Figure 2, the nonlinear substructures are expressed by:

$$\left\{\begin{matrix} G_p(s) = \bar{G}_p(s) + \Delta G_p(s) \\ G_n(s) = \bar{G}_n(s) + \Delta G_n(s) \end{matrix}\right\} \tag{1}$$

where $\{G_p, \Delta G_p, \bar{G}_p\}$ is the physical substructure, the nonlinear term and the linear model, respectively, and $\{G_n, \Delta G_n, \bar{G}_n\}$ is the numerical substructure, nonlinear term and the linear model, respectively. In Figure 2, the output forces from the nonlinear physical substructure and its linear model can be expressed by:

$$\left\{\begin{matrix} f_p(s) = G_p(s) G_{ts}(s) u(s) \\ \bar{f}_p(s) = \bar{G}_p(s) G_{ts}(s) u(s) \end{matrix}\right\} \tag{2}$$

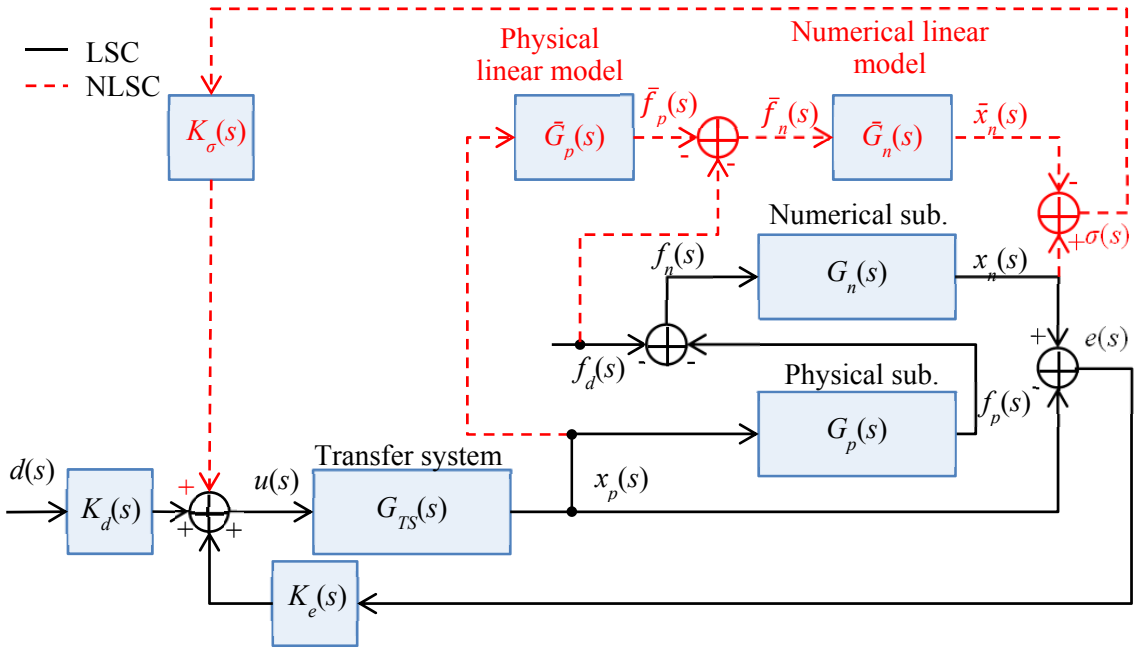

Figure 2. Nonlinear substructuring control, (NLSC)

where f_p and $\bar{f}_p$ are the forces obtained from the physical substructure and its linear model, G_{ts} is the dynamics of transfer system and u is the input signal to the transfer system. Outputs from the numerical substructure and its linear model can be expressed as:

$$\begin{Bmatrix} x_n(s) = G_n(s)\left(-f_p(s) - f_d(s)\right) \\ \bar{x}_n(s) = \bar{G}_n(s)\left(-\bar{f}_p(s) - f_d(s)\right) \end{Bmatrix} \tag{3}$$

Based on equations (2) and (3), the nonlinear signal, σ, shown in Figure 2 is expressed as:

$$\begin{aligned} \sigma(s) &= x_n(s) - \bar{x}_n(s) \\ &= -\left(G_n(s)G_p(s) - \bar{G}_n(s)\bar{G}_p(s)\right)G_{ts}(s)u(s) - \left(G_n(s) - \bar{G}_n(s)\right)f_d(s) \end{aligned} \tag{4}$$

Here, the outputs of the substructures are determined as:

$$\begin{Bmatrix} x_n(s) = \bar{x}_n(s) + \sigma(s) = \bar{G}_1(s)d(s) - \bar{G}_0(s)u(s) + \sigma(s) \\ x_p(s) = \bar{x}_p(s) = \bar{G}_2(s)u(s) \end{Bmatrix} \tag{5}$$

where: $\bar{G}_1(s) = -\bar{G}_n(s)\dfrac{f_d(s)}{d(s)}$, $\bar{G}_0(s) = \bar{G}_n(s)\bar{G}_p(s)G_{ts}(s)$, $\bar{G}_2(s) = G_{ts}(s)$

and $\{\bar{G}_0, \bar{G}_1, \bar{G}_2\}$ is the transfer function set of linear models. Based on equation (5), the error signal between the outputs of two substructures is expressed as:

$$e(s) = x_n(s) - x_p(s) = \bar{x}_n(s) - \bar{x}_p(s) + \sigma(s) = \bar{G}_d(s)d(s) - \bar{G}_u(s)u(s) + \sigma(s) \tag{6}$$

where: $\bar{G}_d(s) = \bar{G}_1(s)$, $\bar{G}_u(s) = \bar{G}_0(s) + \bar{G}_2(s)$.

As shown in equation (6), the error signal is composed of three signals {*e*, *d*, *σ*} related to numerical linear model, physical substructure and nonlinear signal, respectively. Thus, the control signal is proposed as:

$$u(s) = K_d(s)d(s) + K_e(s)e(s) + K_\sigma(s)\sigma(s) \tag{7}$$

Substituting equations (7) into (6), the error signal is rewritten as:

$$e(s) = \frac{\bar{G}_d(s) - \bar{G}_u(s)K_d(s)}{1 + \bar{G}_u(s)K_e(s)}d(s) + \frac{1 - \bar{G}_u(s)K_\sigma(s)}{1 + \bar{G}_u(s)K_e(s)}\sigma(s) \tag{8}$$

The controller transfer functions, K_d and K_σ, need to be determined so that the error becomes zero. According to equation (8), this is ideally achieved by:

$$K_d(s) = \frac{\bar{G}_d(s)}{\bar{G}_u(s)},\ K_\sigma(s) = \frac{1}{\bar{G}_u(s)} \tag{9}$$

When these controller transfer functions are adopted, good control is achievable. In this case, the error feedback action with K_e does not play a key role. However, the error feedback action K_e is important for the compensation of the error generated due to uncertainty and pure time delays.

In the study of LSC in [1], the following equation was found to be a suitable design for K_e:

$$K_e(s) = \frac{1}{\bar{G}_u(s)}\frac{(s+b)}{s^2}\beta \tag{10}$$

Then, the characteristic equation of the closed-loop system described by equation (8) is expressed as:

$$1 + \bar{G}_u(s)K_e(s) = 1 + \frac{(s+b)}{s^2}\beta \tag{11}$$

Based on the classic roots' loci method applied to the open-loop transfer function in equation (11), the controller transfer function K_e can be designed in more detail. Thus, selecting the dominant roots at the break point, $s = -2b$, results in a critically damped closed-loop system with an approximate settling time of $2/b$. Given that the settling time of the transfer system is approximately $4/a$, a suitable design is to ensure that $2/b = 8/a$, i.e. $b = a/4$.

3. Experimentation

NLSC was examined via a substructured test on a nonlinear 2DOF model of a base-isolated structure. Base isolation systems are often used for the prevention of major structural damage under earthquake excitations and hence plasticisation of the superstructure is unlikely to happen in practice. However, for verification of the substructuring test with NLSC, we intentionally designed the superstructure of the base-isolated structure to have low strength, so that it was susceptible to severe damage under moderate earthquake excitation. In this substructured test, the base isolation system

constituted the physical substructure and the rest of the structure constituted the numerical substructure, as shown in Figure 3.

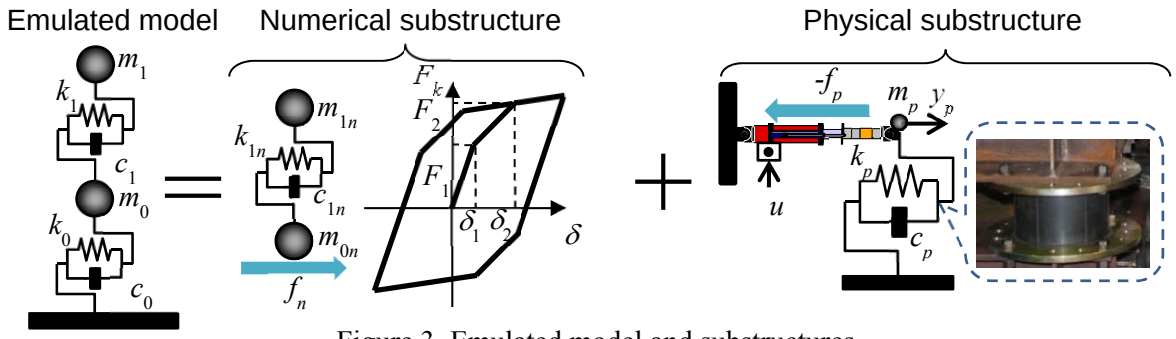

Figure 3. Emulated model and substructures

2.1 Configuration

The emulated 2-DOF dynamics, subjected to an earthquake excitation in Figure 3, are expressed by:

$$\begin{Bmatrix} m_1\left(\ddot{x}_1(t)+\ddot{d}(t)\right)+f_{c1}\left(\dot{x}_1,\dot{x}_0,t\right)+f_{k1}\left(x_1,x_0,t\right)=0 \\ m_0\left(\ddot{x}_0(t)+\ddot{d}(t)\right)+f_{c0}\left(\dot{x}_0,t\right)+f_{k0}\left(x_1,x_0,t\right)-f_{c1}\left(\dot{x}_1,\dot{x}_0,t\right)-f_{k1}\left(x_1,x_0,t\right)=0 \end{Bmatrix} \tag{12}$$

where d is the ground motion (i.e. earthquake excitation) and $\{x_i,\ m_i,\ f_{ci}, f_{ki}\}$, $(i = 0,1)$, is the relative displacement, mass, damping force and restoring force in the i^{th} storey. The numerical and physical substructure dynamics are then expressed by:

$$\begin{Bmatrix} m_{1n}\left(\ddot{x}_{1n}(t)+\ddot{d}(t)\right)+f_{c1n}\left(\dot{x}_{1n},\dot{x}_{0n},t\right)+f_{k1n}\left(x_{1n},x_{0n},t\right)=0 \\ m_{0n}\ddot{x}_0(t)+m_{1n}\left(\ddot{x}_{1n}(t)+\ddot{d}(t)\right)=f_n(t)\left(=-f_p(t)-m_0\ddot{d}(t)\right) \end{Bmatrix} \tag{13}$$

$$m_p\ddot{x}_p(t)+f_{pc}\left(\dot{x}_p,t\right)+f_{pk}\left(x_p,t\right)=f_p(t) \tag{14}$$

where $m_{0n}= m_0-m_p$, $m_{1n}= m_1$ and $\{f_n, x_{0n}, m_{0n}\}$ is the force, relative displacement and mass of the ground floor (GF) in the numerical substructure, $\{x_{1n},\ m_{1n},\ f_{c1n},\ f_{c1n}\}$ is the relative displacement, mass, damping force and restoring force of the 1st (1F) storey in the numerical substructure and $\{f_p, x_p, m_p, f_{pc}, f_{pk}\}$ is the relative displacement, mass, damping force and restoring force of the physical substructure, respectively.

Linear models of the substructures are based on linearization of the stiffness and damping terms, as follows:

$$\begin{Bmatrix} \bar{m}_{1n}\left(\ddot{\bar{x}}_{1n}(t)+\ddot{d}(t)\right)+\bar{c}_{1n}\left(\dot{\bar{x}}_{1n}(t)-\dot{\bar{x}}_{0n}(t)\right)+\bar{k}_{1n}\left(\bar{x}_{1n}(t)-\bar{x}_{0n}(t)\right)=0 \\ \bar{m}_{0n}\ddot{\bar{x}}_{0n}(t)+\bar{m}_{1n}\left(\ddot{\bar{x}}_{1n}(t)+\ddot{d}(t)\right)=\bar{f}_n(t)\left(=-\bar{f}_p(t)-\bar{m}_0\ddot{d}(t)\right) \end{Bmatrix} \tag{15}$$

$$\bar{m}_p\ddot{\bar{x}}_p(t)+\bar{c}_p\dot{\bar{x}}_p(t)+\bar{k}_p\bar{x}_p(t)=\bar{f}_p(t) \tag{16}$$

where $\bar{m}_p = m_p$, $\bar{m}_{0n} = m_{0n}$, $\bar{m}_{1n} = m_{1n}$, $\bar{c}_{1n} = c_{1n}$. In addition, $\{\bar{f}_n, \bar{x}_{0n}, \bar{m}_{0n}\}$ is the force, relative displacement and mass of the GF storey in the numerical linear model, $\{\bar{x}_{1n}, \bar{m}_{1n}, \bar{c}_{1n}, \bar{k}_{1n}\}$ is the relative displacement, mass, damping coefficient and stiffness coefficient of the 1F storey in the numerical linear model and $\{\bar{f}_p, \bar{x}_p, \bar{m}_p, \bar{c}_p, \bar{k}_p\}$ is the force, relative displacement, mass, damping coefficient and stiffness coefficient of the physical linear model.

In the Laplace domain, the outputs of the physical and numerical substructures are then determined as:

$$\left\{\begin{array}{l} x_n(s) = \bar{x}_n(s) + \sigma(s) = \bar{G}_1(s)\ddot{d}(s) - \bar{G}_0(s)u(s) + \sigma(s) \\ x_p(s) = \bar{G}_2(s)u(s) \end{array}\right\} \tag{17}$$

where:
$$\left\{\begin{array}{l} \bar{G}_1(s) = -\dfrac{(\bar{m}_p + \bar{m}_{0n})\bar{m}_{1n}s^6 + \bar{c}_{1n}(\bar{m}_p + \bar{m}_{0n} + \bar{m}_{1n})s^5 + \bar{k}_{1n}(\bar{m}_p + \bar{m}_{0n} + \bar{m}_{1n})s^4}{\bar{m}_{0n}\bar{m}_{1n}s^6 + \bar{c}_{1n}(\bar{m}_{0n} + \bar{m}_{1n})s^5 + \bar{k}_{1n}(\bar{m}_{0n} + \bar{m}_{1n})s^4} \\ \bar{G}_0(s) = \dfrac{(\bar{m}_p s^2 + \bar{c}_p s + \bar{k}_p)(\bar{m}_{1n}s^2 + \bar{c}_{1n}s + \bar{k}_{1n})}{\bar{m}_{0n}\bar{m}_{1n}s^4 + \bar{c}_{1n}(\bar{m}_{0n} + \bar{m}_{1n})s^3 + \bar{k}_{1n}(\bar{m}_{0n} + \bar{m}_{1n})s^2} \dfrac{a}{s+a} \\ \bar{G}_2(s) = \dfrac{a}{s+a} \end{array}\right\}$$

Note that base-isolated structures are normally tested using the recorded acceleration from an earthquake site, hence equation (17) is also written for the ground motion acceleration. Based on the general transfer functions G_0, G_1 and G_2 in equation (17), the controller transfer functions will be designed for each testing condition, as shown below.

2.2 Test conditions

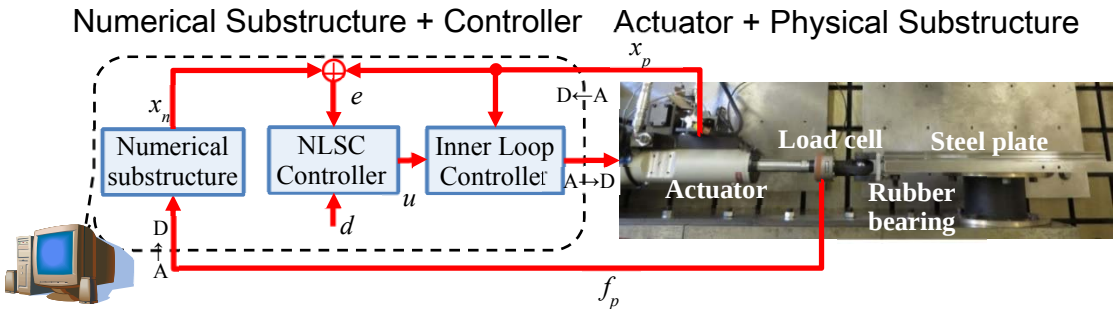

Figure 4. Test rig.

The schematic representation of the test rig in Figure 4 comprises a ±25 kN force, ±120.0 mm stroke servohydraulic actuator and a proprietary inner-loop discrete-time controller (together known as the transfer system), plus a connecting steel plate and a bearing made of natural rubber (the physical substructure). In addition to the substructure control signal, the actuator was configured to additively generate earthquake ground excitations to the rubber bearing. The diameter and height of the rubber bearing were 200.0 mm and 125.0 mm, respectively, and the measured mass of the steel plate was 115 kg. Rigid connections ensured that the outputs from the LVDT displacement transducer and load cell attached to the actuator were equivalent to the displacement and force applied to the rubber bearing. DSS was implemented as an outer-loop configuration using *dSPACE* 1104 hardware, operating with a

sampling interval of 1.0 ms.

Identification tests were conducted on the physical substructure and transfer system using a band-limited white noise excitation between 0.02×2π rad/s and 100.0×2π rad/s, of time duration 120.0 s and a sampling interval of 1.0 ms. Following system identification, the parameters of the physical substructure were determined as m_p = 114.3 kg, c_p = 354.6 Ns/m and k_p = 158.4 kN/m, resulting in a natural frequency and damping ratio of ω_p = 5.91×2π rad/s and ζ_p = 0.0415. Similarly, the dynamics and pure time-delay of the transfer system were identified as a = 75.0 s^{-1} and τ = 6.0 ms.

The numerical substructure parameters were selected as m_{0n} = 9885 kg, m_{1n} = 10000 kg, k_{1n} = 158.4 kN/m and c_{1n} = 354.6 Ns/m, so that the emulated system had homogenous parameters for the mass, stiffness and damping for each DOF, and its first natural frequency was 0.393 Hz in the elastic range. The nonlinear hysteresis incorporated into the numerical substructure, as shown in Figure 3, was set to decrease to one-half of the initial stiffness at the inter-storey drift δ_1 (= 15 mm) and to one-tenth of the initial value at the inter-storey drift δ_2 (= 30 mm).

2.3 Test results

Substituting the above-mentioned parameters $\{m_p, c_p, k_p, m_{0n}, m_{1n}, k_{1n}, c_{1n}\}$ into equation (17) as the linear model parameters, the input signal generated by NLSC to the transfer system was determined with the control law in equation (18) and the corresponding transfer functions shown below:

$$u(s) = K_{\ddot{d}}(s)\ddot{d}(s) + K_e(s)e(s) + K_{\ddot{\sigma}}(s)\ddot{\sigma}(s) \tag{18}$$

where:
$$\left\{\begin{array}{l} K_{\ddot{d}}(s) = \dfrac{\bar{G}_1(s)}{\bar{G}_0(s)+\bar{G}_2(s)} = -\dfrac{0.01333s^3+1.001s^2+0.4995s+32}{s^4+0.1092s^3+48s^2+1.165s+256} \\ K_{\ddot{\sigma}}(s) = \left(\dfrac{1}{\bar{G}_0(s)+\bar{G}_2(s)}\right)\left(\dfrac{1}{s^2}\right) = \dfrac{0.01318s^3+0.9895s^2+0.4966s+31.82}{s^4+0.1092s^3+48s^2+1.165s+256} \\ K_e(s) = \left(\dfrac{1}{\bar{G}_0(s)+\bar{G}_2(s)}\right)\left(\dfrac{s+b}{s^2}\right)\beta = K_{\ddot{\sigma}}(s)(s+b)\beta \end{array}\right\}$$

Here, the parameter b used in K_e was set to b = 18.75, based on the design of $b = a/4$. In addition, the parameter β was designed to be 100, based on the classic roots' loci method. As a benchmark, K_e and $K_{\ddot{d}}$ were taken as the controller transfer functions of LSC.

Substructuring tests based on NLSC and LSC were conducted with a Japan Meteorological Agency Kobe ground motion, which was recorded at the 1995 Kobe Earthquake. The amplitude of the ground motion was scaled to 30% of the original, due to the limitation of the maximum stroke in the actuator. In the substructured tests, LSC and NLSC maintained stability as shown in Figures 5(a) and 6(a), and the maximum error between x_{n1} and x_p was recorded as 0.5 mm with NLSC and 1.2 mm with LSC. Although NLSC generated more accurate responses than LSC, both methods were found to be entirely acceptable in experimentation.

However, the substructured syntheses were based upon accurate values of the physical substructure parameters, although these parameters would in general be unknown in advance of a practical DSS test. Therefore, in practice, these parameters would be estimated only approximately. In order to demonstrate such a case, we also conducted a test using controller transfer functions based upon poor estimations of physical substructure's parameters. A relatively extreme case was considered - the damping and stiffness terms in the physical substructure, k_p and c_p, were estimated to be ten times the originally identified values. Then, substituting $\{m_p, 10c_p, 10k_p, m_{1n}, m_{2n}, k_{2n}, c_{2n}\}$ into equation (17), the signal generated by NLSC to the transfer system was determined as:

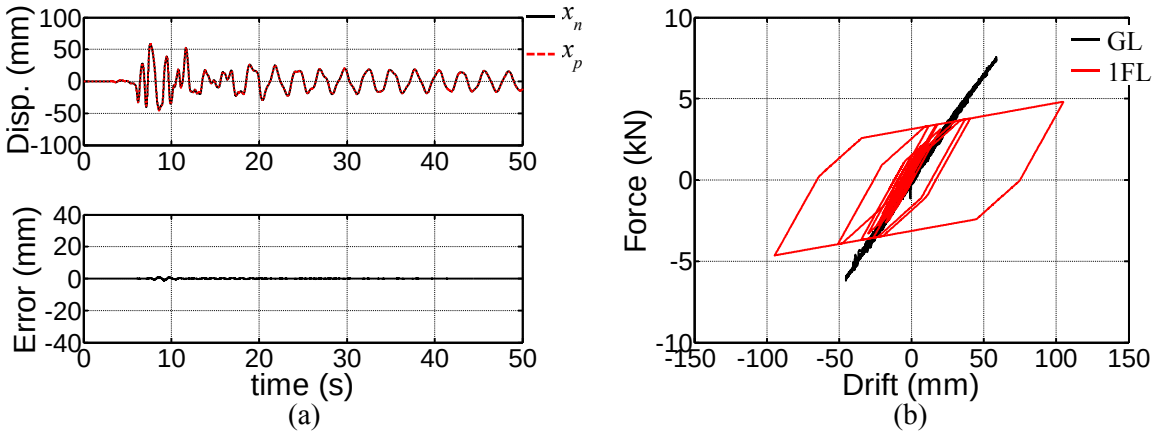

Figure 5. Substructured test with LSC, based on accurate estimation of the physical substructure parameters; (a) time history, (b) hysteresis.

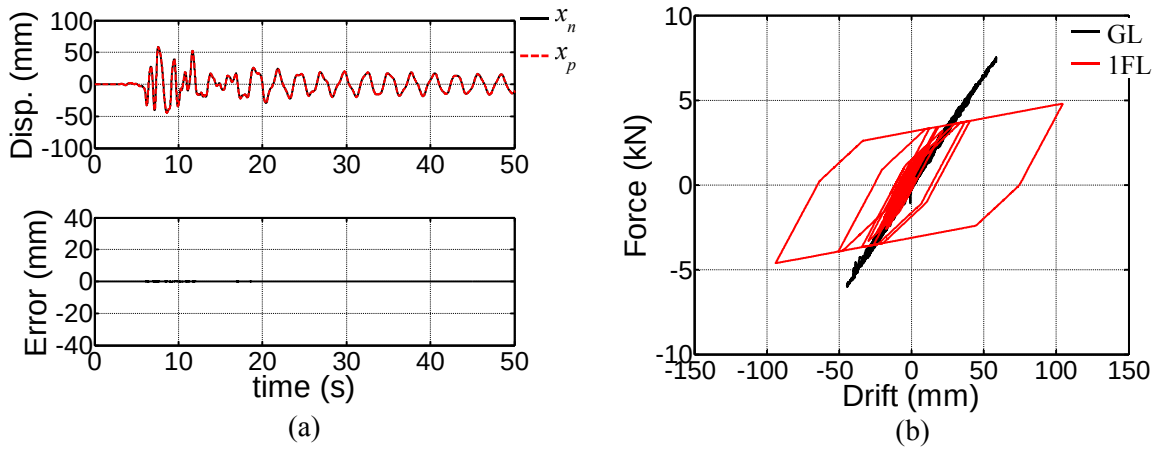

Figure 6. Substructured test with NLSC, based on accurate estimation of the physical substructure parameters; (a) time history, (b) hysteresis.

$$u(s)=K_{\ddot{d}}(s)\ddot{d}(s)+K_e(s)e(s)+K_{\ddot{\sigma}}(s)\ddot{\sigma}(s) \tag{19}$$

where:
$$\begin{cases} K_{\ddot{d}}(s)=\dfrac{\bar{G}_1(s)}{\bar{G}_0(s)+\bar{G}_2(s)}=-\dfrac{0.01333s^3+1.001s^2+0.4995s+32}{s^4+0.4368s^3+192s^2+11.65s+2560} \\ K_{\ddot{\sigma}}(s)=\left(\dfrac{1}{\bar{G}_0(s)+\bar{G}_2(s)}\right)\left(\dfrac{1}{s^2}\right)=\dfrac{0.01318s^3+0.9895s^2+0.4966s+31.82}{s^4+0.4368s^3+192s^2+11.65s+2560} \\ K_e(s)=\left(\dfrac{1}{\bar{G}_0(s)+\bar{G}_2(s)}\right)\left(\dfrac{s+b}{s^2}\right)\beta=K_{\ddot{\sigma}}(s)(s+b)\beta \end{cases}$$

and b = 18.75 and β = 100; [1]. Again, K_e and $K_{\ddot{d}}$ were used as the controller transfer functions for

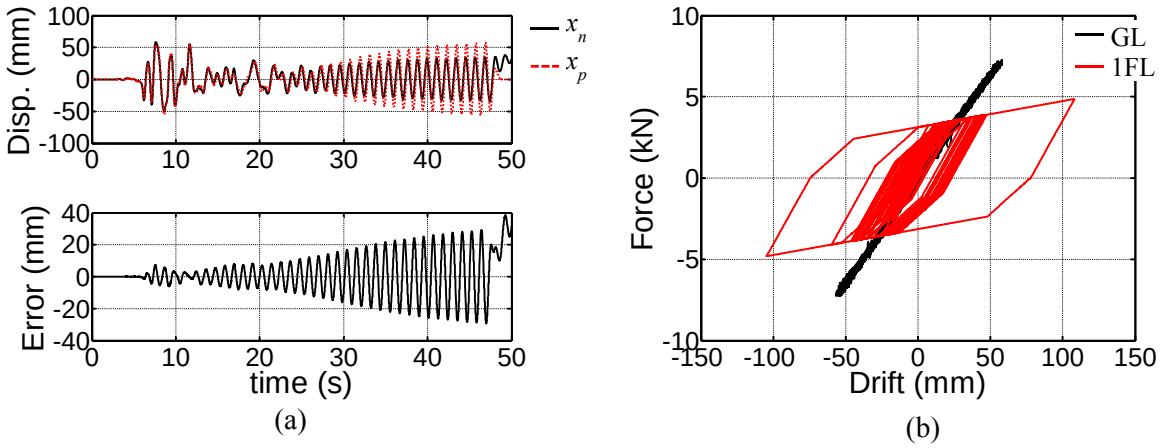

(a) (b)

Figure 7. Substructured test with LSC, based on poor estimation of the physical substructure parameters; (a) time history, (b) hysteresis.

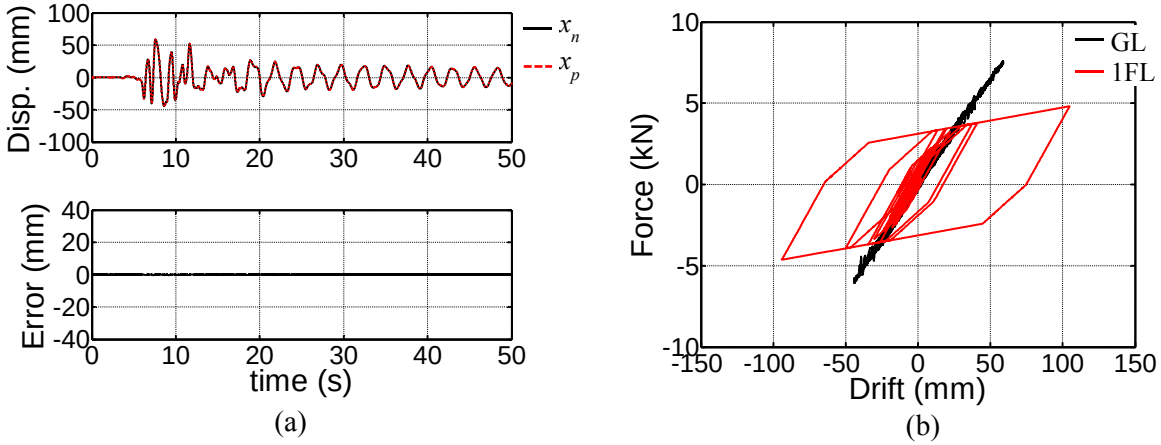

(a) (b)

Figure 8. Substructured test with NLSC, based on poor estimation of the physical substructure parameters; (a) time history, (b) hysteresis.

LSC.

Substructuring tests based on NLSC and LSC were conducted with the same ground motion as used in the first experiments. According to Figures 7(a) and 8(a), LSC failed to maintain stability in the case of the poorly estimated parameters, whilst NLSC was able to do so, achieving good responses.

3. Conclusions

The conclusions obtained in this work are now summarised in brief. NLSC was developed as a generalised form of LSC, based upon the NSBC method. Substructuring tests on a nonlinear 2DOF system with a rubber bearing and a nonlinear superstructure were implemented for the examination of NLSC. In the substructured test, where the properties of physical substructure were well known, NLSC and LSC achieved accurate output responses of the substructures, although the errors due to LSC were slightly larger than those of NLSC. However in the case of poorly estimated physical substructure parameters, LSC became unstable whilst NLSC achieved very acceptable results.

References

[1] Enokida R Stoten D and Kajiwara K 2015 Stability analysis and comparative experimentation for two substructuring schemes, with a pure time delay in the actuation system *J. Sound Vib.* **346** pp 1–16
[2] Carrison JE Spencer BF and Phillips BM 2009 Real-time hybrid simulation for structural control performance assessment *Earthq. Eng. Eng. Vib.* **8**(4) pp 481–492
[3] Horiuchi T Inoue M Konno T and Namita Y 1999 Real-time hybrid experimental system with actuator delay compensation and its application to piping system with energy absorber *Earthquake Eng. Struc.***28**(10) pp 1121–1141
[4] Darby AP Blakeborough A and Williams MS 1999 Real-time substructure tests using hydraulic actuators *Journal of Engineering Mechanics* **125**(12) pp 1133–1139
[5] Ahmadizadeh M Mosqueda G and Reihorn AM 2008 Compensation of actuator delay and dynamics for real-time hybrid structural simulation *Earthquake Eng. Struc.* **37**(1) pp 21–42
[6] Mosqueda G Stajodinovic B and Mahin S 2007 Real-time error monitoring for hybrid simulation Part II: structural response modification due to errors *J. Struct. Eng.-ASCE* **133**(8) pp 1109–1117
[7] Wallace MI Wagg DJ Sieber J and Neild SA 2005 An adaptive polynomial based forward prediction algorithm for multi-actuator real-time dynamic substructuring *Philos. T. Roy. Soc. A* **461**(2064) pp 3807–3826
[8] Carrion J and Spencer B 2007 Model-based Strategies for Real-time Hybrid Testing; Newmark Structural Engineering Laboratory Report Series; Urbana, IL: University of Illinois at Urbana-Champaign.
[9] Gao X, Castaneda NE and Dyke SJ 2013 Real time hybrid simulation: from dynamic system, motion control to experimental error *Earthquake Eng. Struc.* **42**(6) pp. 815–832
[10] Stoten DP and Hyde RA 2006 Adaptive control of dynamically substructured systems: the single-input single-output case *P. I Mech. Eng. I.-J. Sys.* **220**(2) pp 63–79
[11] Stoten DP 2014 A comparison of hybrid and DSS schemes for substructured system testing, *MOVIC 2014* Japan Society of Mechanical Engineers, Hokkaido, Japan
[12] Enokida R Takewaki I and Stoten D 2014 A nonlinear signal-based control method and its applications to input identification for nonlinear SIMO problems *J. Sound Vib.* **333**(24) pp 6607–6622